Analytical Techniques for Laser Remote Sensing with a Super-Continuum White Light Laser

Joseph Begnoche - Masters of Science in Electrical Engineering

***Abstract* - Initial laboratory experiments have been concluded to investigate the abilities of a white light super continuum laser beam generated by a femtosecond laser pulse, for its application in atmospheric remote sensing. The spectral components of this PSU white light laser, which range from 200 nm to about 1700 nm, can be used as the source for long path spectrometer measurements of atmospheric constitutes. Before the white light laser technology can be considered a robust means of atmospheric remote sensing, a well developed method of the data analysis for detection and quantification must be developed. This study will explore two methods that have been previously proposed in the literature for quantification techniques for white light laser data, and a new method will be presented that uses data from recent laboratory experiments. A newly prepared femtosecond pulsed laser has been used for detection of water vapor absorption features in the region of 1350 nm to 1420 nm. The sub-nanosecond laser pulses from a passively Q switched microchip laser are coupled into a 2 cm long photonic crystal fiber to generate super-continuum white light. The white light generated is collimated and propagates along a path of 20 meters in air. The transmitted spectrum is collected and recorded by an optical spectrum analyzer. The laboratory has a controlled atmosphere and the relative humidity and temperature were recorded using a sling psychrometer.**

I. INTRODUCTION

Laser remote sensing has been the means of molecular and particle detection and quantification of the atmosphere since the late 1960s [1]. Since its beginnings lidar, light detection and ranging, techniques and methods have been developed and integrated into the field of atmospheric research. Lidar exploits the physics of light and particle interactions for detection and quantification. These interactions are categorized into eight different processes for lidar operation; Rayleigh scattering, Mie scattering, Raman scattering, resonance scattering, fluorescence, absorption, differential absorption, and differential scattering [1]. Lidar systems are used in applications that demand concentration meas-

urements of major and minor constitutes, evaluation of thermal, structural, and dynamical properties of the atmosphere, threshold detection of biologically harmful gases, and spectral fingerprinting of specific targets. These basic abilities of a lidar system have enhanced the measuring capability for many industrial and research applications. To take advantage of the processes of light and matter interaction three basic lidar techniques and equations have been derived. These three basic lidar equations, developed and described by Measures [1], are the scattering form of the lidar equation, the DIAL (Differential Absorption Lidar) equation, and the fluorescent form of the lidar equation. These lidar equations provide different analytical techniques to extract the quantity of interest from the data of a lidar system. For example the DIAL equation is given by Measures [1] as,

$$\int_0^{R_T} N(R)dR = \frac{1}{2 \cdot \sigma_A(\lambda_o : \lambda_W)}\left[\ln\left\{\frac{E(\lambda_W, R_T)}{E(\lambda_o, R_T)}\right\}\right], \tag{1}$$

where,

$N(R)$	is the number density of the molecule of interest range R,
R_T	is the total distance of the absorption path,
$E(\lambda_W, R_T)$	is the detected energy at the absorption wavelength of the molecule,
$E(\lambda_o, R_T)$	is the detected energy at the off wavelength,
$\sigma_A(\lambda_o : \lambda_W)$	is the differential absorption cross section.

A DIAL system typically uses two laser wavelengths for a measure of the integrated concentration along a path. Equation (1) assumes that the total attenuation coefficient, not including the selected absorption features, along the path is the same for both laser wavelengths. This is typically done when the two wavelengths are carefully chosen such that the ‘on’ wavelength is at an absorption feature of the molecule of interest and the ‘off’ wavelength is near the ‘on’ wavelength but in a region free of the absorption of the molecule. The required closeness of the ‘on’ and ‘off’ wavelengths is dependant on the scattering along the path. Typically because of the laser wavelengths used and the size of the scatters the scattering is said to be Rayleigh scattering which can be assumed equal for very close wavelengths.

The DIAL equation and the method above describing the 'on' and 'off' wavelengths is referred to as the DIAL technique. Other techniques have been developed for Rayleigh scattering and Raman scattering lidar systems using the scattering form of the lidar equation and for fluorescence lidar systems using the resonance scattering form of the lidar equation. These different lidar systems examine very different processes and apply different analysis, but are very similar in system components. A basic lidar system consists of a transmitter and receiver. The transmitter uses laser radiation selected for a specific wavelength for the particular application. The receiver and detectors mainly consists of a telescope to focus the returned light energy that passes though a band pass filtering system to remove unwanted wavelengths before it goes into a photodetector that is usually sampled and connected to a computer. Currently, the lasers used for the transmitters range in wavelengths from the ultraviolet through the visible and into the infrared wavelengths. The laser can be considered the heart of a lidar system; its wavelengths and power define what molecule can be detected. In an effort to enhance the functionality of a lidar system, this paper considers the use of a broadband white light laser for the transmitter. Supercontinuum white light lasers can provide for multiple molecule and particle detection in the atmosphere. The large bandwidth provided by a white light laser permits examination of large spectral regions to measure many different molecules present along a path. These capabilities in a lidar transmitter will allow lidar systems to detect the different processes of light and mater interaction as described above and will expand the functionality of a lidar system.

White light lasers have been shown to be produced from the spectral broadening of femtosecond laser pulses using a fiber with photonic-crystal cladding (Knight et al. [5]). Photonic-crystal cladding consists of a 2D periodic array of closely packed hollow silica fibers. The periodic arrangement of air holes in the cladding produces a transmission spectrum that displays photonic band gaps. Photonic band gap cladding (PBG) has also been referred to holey fibers and allow for single-mode propagation with a broad spectral range [6].

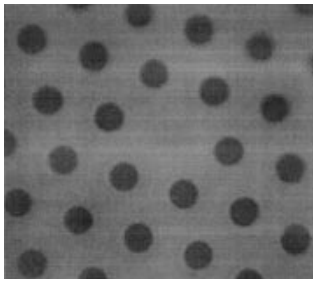

Figure 1: A microscopic image of a cut of a holey fiber with PBG cladding (Fedotov et al. [6]).

Another method for laser pulse broadening to produce a white light laser beam was demonstrated by the Teramobile lidar system, a French-German research project. The Teramobile system has been fully described in the scientific literature of Wille et al. [7]. It has a peak power of 5 terawatts, a pulse duration of 100 femtoseconds and propagates in the air to induce a change to the refractive index of air. The refractive change causes a focusing-effect known as the Kerr effect. This focusing is balanced by diffraction caused by the plasma created by the strong electric fields of the high-intensity pulse, and results in a dynamic equilibrium, with self-guided filaments [7].

Figure 2: Photograph of a self-guided filament induced in air by a high-power, infrared (800 nm) laser pulse [16].

The Teramobile system has provided much of the initial emphasis on the use of a high power white light lidar system. The high power capability gives the Teramobile team an ability to investigate many nonlinear effects associated with short pulse propagation in the atmosphere. Teramobile data analysis has been provided by Mejean et al [8] to show data analysis techniques to extract particle size and relative humidity of clouds. These analysis techniques are designed to the nonlinear interactions of the terawatt pulsed laser.

The femtosecond laser system has been built in the Penn State University Ultrafast optics laboratory using the photonic-crystal cladding technology (Shi et al. [17]). This same method for supercontinuum generation has been described and implemented by Knight et al. [5]. Sub-nanosecond laser pulses from a passively Q switched microchip laser are coupled into a 2 cm long photonic crystal fiber [9]. Figures 3, 4 and 5 show the output spectrum of the PSU white light laser.

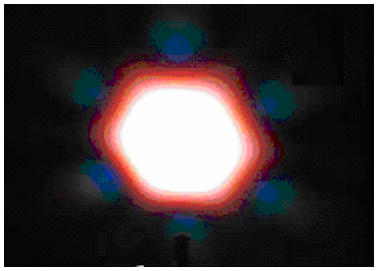

Figure 3: The far field pattern of the supercontinuum white light generated from a photonic crystal fiber [9]

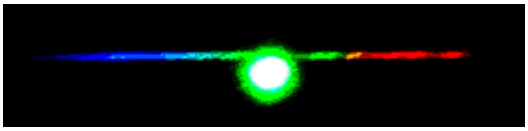

Figure 4: The rainbow observed after the collimated white light passes through a prism [9].

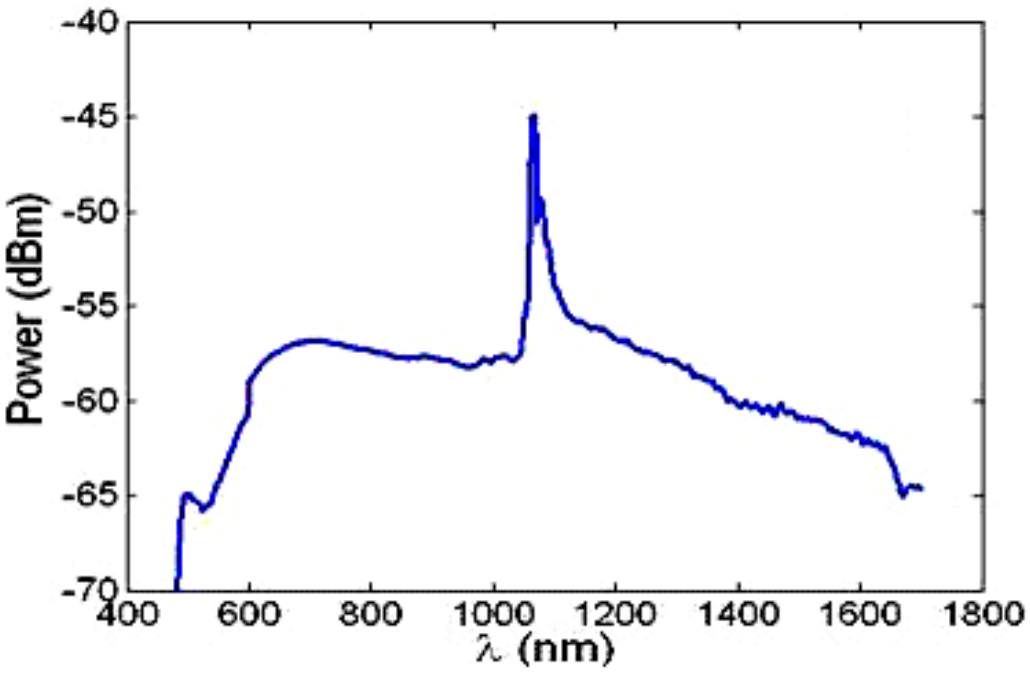

Figure 5: The spectrum of the supercontinuum generated from sub-nanosecond laser pulses [9].

The production of this supercontinuum white light spectrum has provided an opportunity to develop collaboration between the Penn State Lidar laboratory and the Ultrafast Optics Laboratory to perform measurements in the area of atmospheric remote sensing. An initial measurement was performed to measure the absorption of water vapor over 70 nm in the infrared spectrum, from 1350 nm to 1420 nm. This experiment is our initial exploit using the white light laser as the transmitter of a lidar sys-

tem. The result presented here will provide an analysis technique for future use of such a lidar system. This investigation considers two analysis techniques previously reported and gives an explanation of a new analysis approach to extract the relative humidity.

II. BACKGROUND

A brief description of the laboratory experiment that was conducted to extract the relative humidity measurement from path absorption is provided.

A. Cross Section and Spectral Lines

Spectroscopy is the discipline that deals with the study of the absorption and emission of electromagnetic radiation by atoms and molecules. The spectral lines in molecular spectroscopy are associated with the emission or absorption of a photon when the energy state of a molecule changes [10]. Molecular spectroscopy is different from atomic spectroscopy by the more complex spectral features due to the vibrational, rotational, stretching and bending motions. These energy states exist only in molecules due to the bonds between the atoms. The spectral features of the molecule are due to interactions with the electromagnetic field, and are explained by Atkins [10]. To absorb or emit a photon of frequency ν, it must possess an oscillating dipole at that frequency. For emission and absorption spectra, this is expressed quantum mechanically in terms of a transient dipole moment. The intensities of the spectra are proportional to the square of the transition dipole moment and are given by the Einstein coefficient for stimulated absorption. The cross section of the interaction process is related to the intensity of the transition (Atkins [10]). The cross sectional values for simple molecules have been calculated (HITRAN database [11]). The calculations of these cross sections are complex and are detailed in the original HITRAN report by McClatchey et al. [11]. The dependencies and shapes of the molecular spectral lines are obtainable from the HITRAN model, our particular interest here is for water in the wavelength range of 1350 nm to 1420 nm, or wavenumbers from about 7050 cm^{-1} to 7400 cm^{-1}. The dependences of the line shapes are shown in Equation (2) to be frequency, temperature and pressure. The line widths are limited by the natural lifetime of the energy state of the molecule and the line shape is a Lorentz function,

$$f\left(\nu,\nu_{\eta\eta'},T,p\right)=\frac{\gamma\left(p,T\right)}{\pi\gamma\left(p,T\right)^2+\pi\left(\nu-\nu^*_{\eta\eta'}\right)^2}\,, \tag{2}$$

where,

$\gamma\left(p,T\right)$ is the FWHM as a function of pressure and temperature,

ν is the frequency,

$\nu^*_{\eta\eta'}$ is pressure shifted frequency.

The term $\nu^*_{\eta\eta'}$ is given as,

$$\nu^*_{\eta\eta'}=\nu_{\eta\eta'}+\delta\cdot p\,, \tag{3}$$

where,

$\nu_{\eta\eta'}$ is the line transition frequency,

δ is the air broadened pressure shift given in HITRAN.

The cross section values are given as,

$$\sigma\left(\nu,p,T\right)=S_{\eta\eta'}\left(T\right)\cdot f\left(\nu,\nu_{\eta\eta'},T,p\right), \tag{4}$$

where,

$\sigma\left(\nu,p,T\right)$ is the cross section as a function of frequency, pressure and temperature,

$S_{\eta\eta'}\left(T\right)$ is the cross section coefficient as a function of temperature (HITRAN database gives for T = 296K).

The broadening that gives spectral line the Lorentz line shape is also called ‘uncertainty broadening’ (Atkins [10]). No excited state has infinite lifetime; therefore, all state are subject to lifetime broadening, the shorter the lifetime of the state then the broader the spectral line. This relationship is given by,

$$\delta E\approx\frac{\hbar}{\tau}, \tag{5}$$

where,

δE is the energy broadening,

$\hbar$ is Planks constant,

τ is the lifetime of the transition.

The energy spread is expressed in wavenumber as $\delta E = hc\delta\nu$. The natural linewidth is an intrinsic property of the transition, and cannot be changed by modifying the conditions (Atkins [10]). The HI-TRAN database gives the values of the cross sections as a function of wavenumber. Figure 6 shows the cross section for water in the wavelength range of interest.

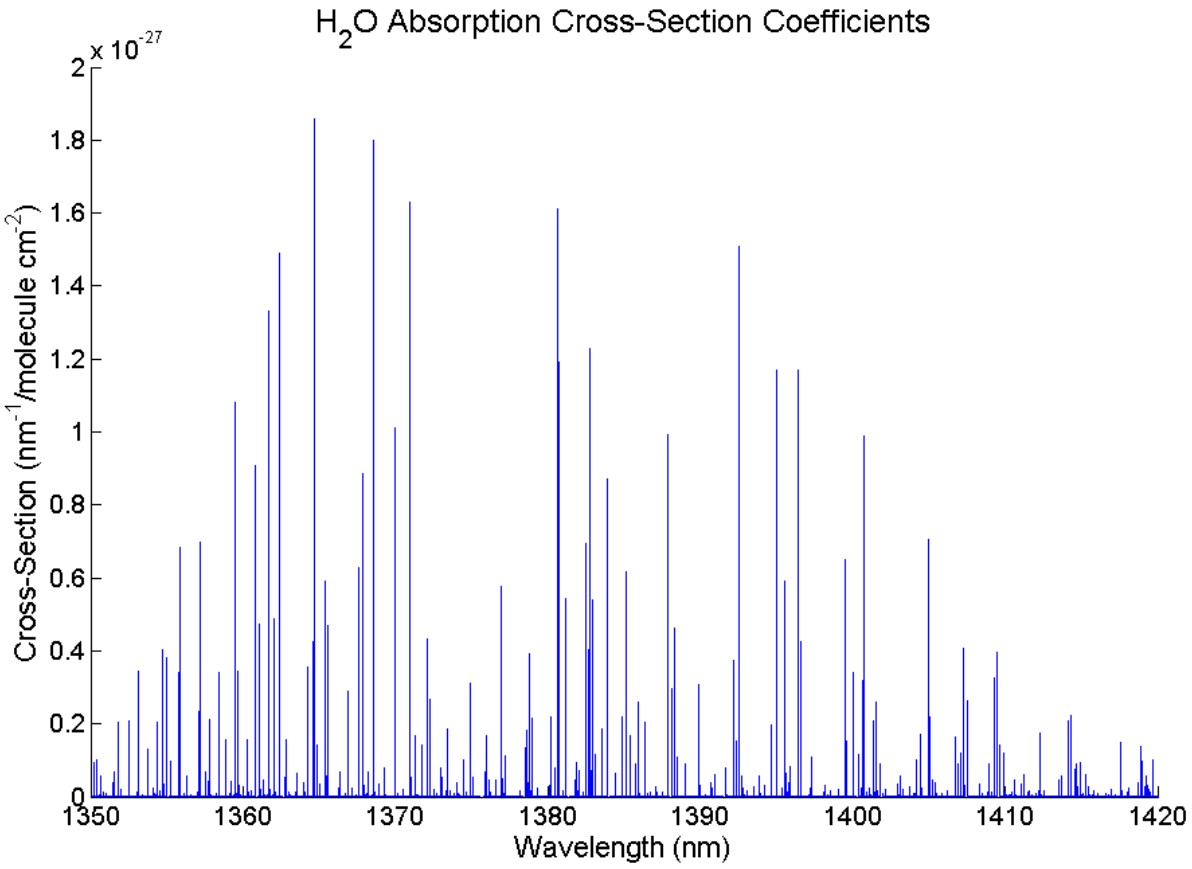

Figure 6: Cross section coefficients plotted for water using the HITRAN database.

This plot does not consider the broadening of the spectral lines, but it does show the behavior of the molecule at different wavelengths. Figure 7 shows a single line with the line-broadened absorption for the water feature at 502.26 cm^{-1}.

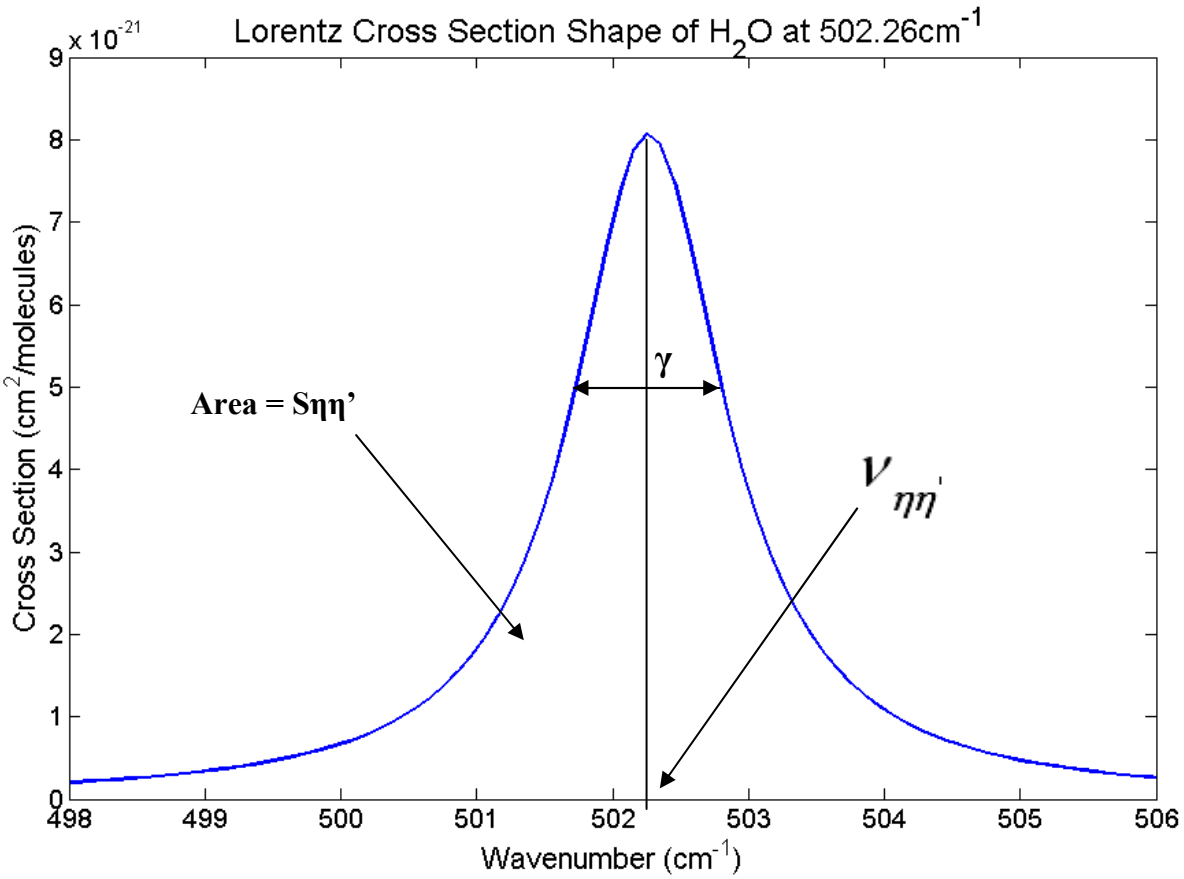

Figure 7: A single Lorentz function for a temperature broadened cross section.

The parameters explained in the equations above are shown on the plot and are given in the HITRAN database. The width shown for a single absorption line is calculated for each line that is shown in Figure 6 and the result is shown in Figure 8.

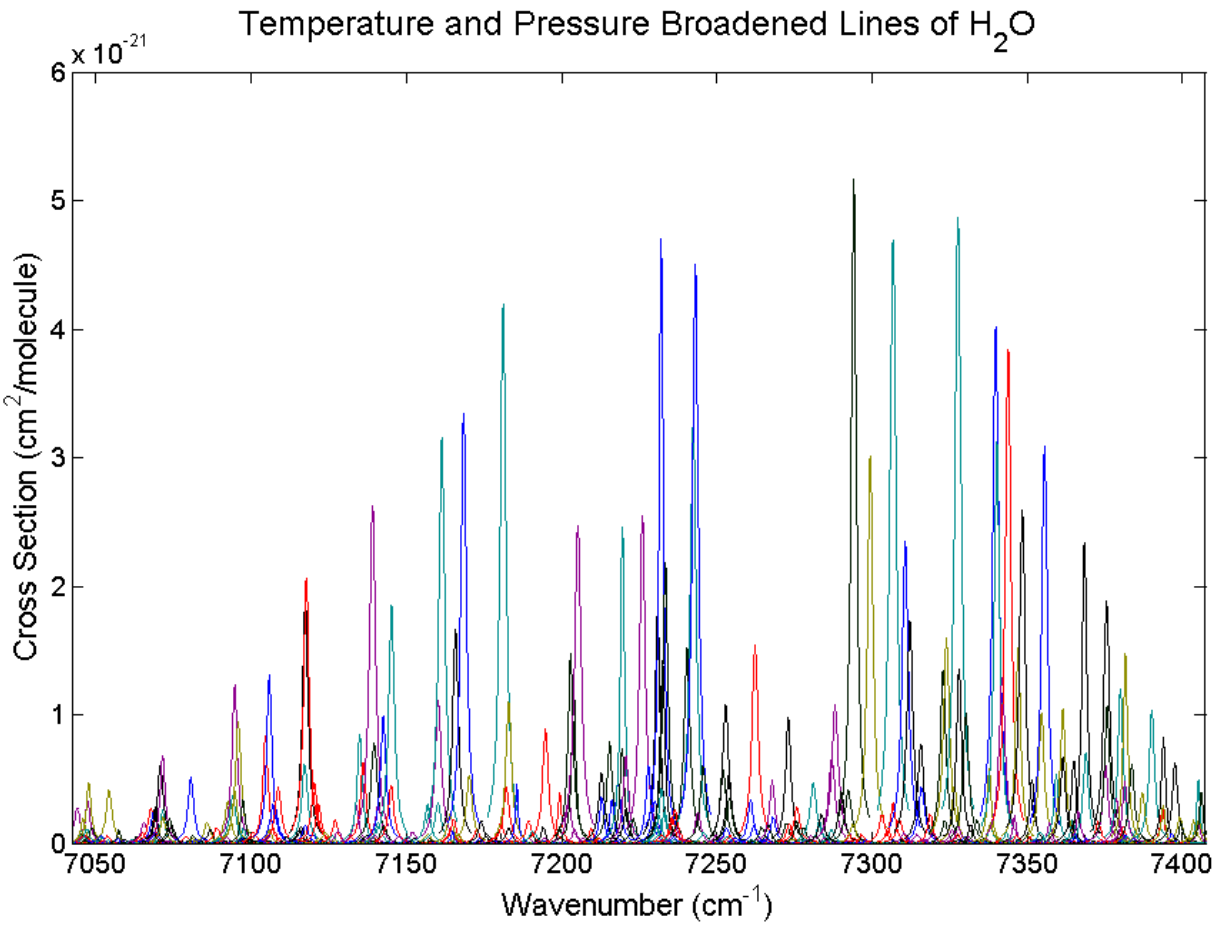

Figure 8: The calculated broadening for the water absorption lines.

Figure 9 shows a smaller range to see the Lorentz function for different frequencies.

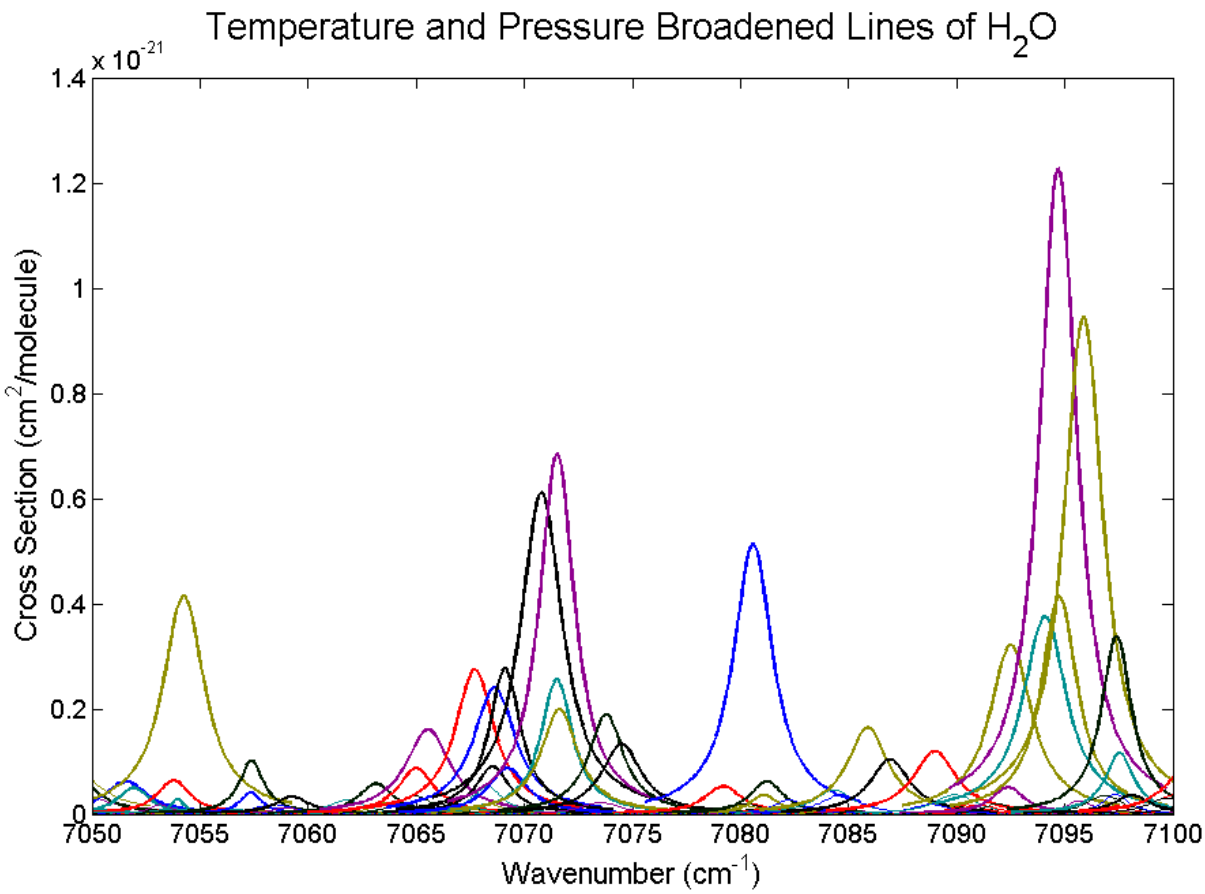

Figure 9: More detailed plot of the many Lorentz lines of the absorption by water.

In Figure 9, the broadened line overlapping is clearly observed. These features are consequently added together to form the resulting absorption spectrum of water shown in Figure 10.

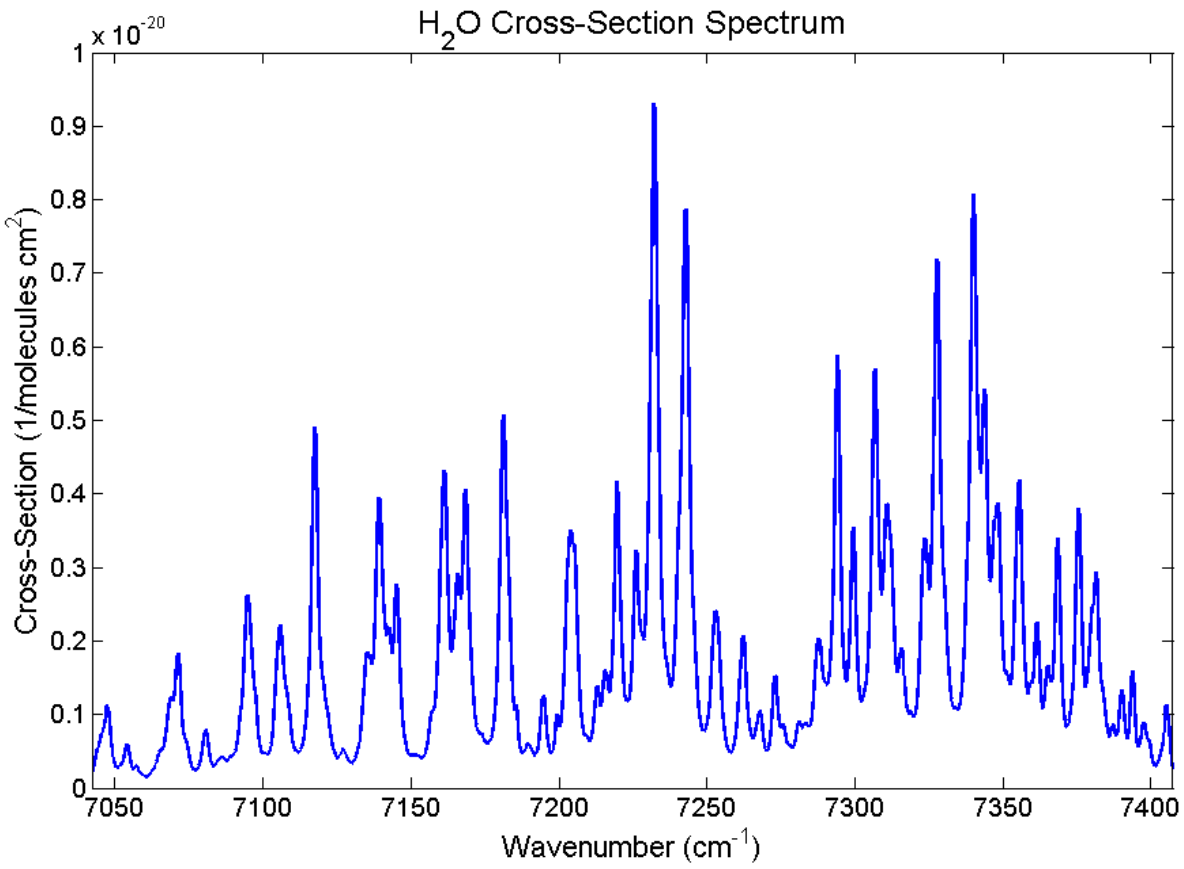

Figure 10: The summation of all the Lorentz functions that make up the water absorption in the spectral range of interest.

These figures have been generated by using the HITRAN database. The cross section shown in Figure 10 gives the absorption characteristics for water for the particular region of the spectrum of interest. This relationship dictates the effects of impinging electromagnetic radiation will have on a water molecule. The next section will consider the effects that the water molecule will have on the impinging radiation and it will also consider multiple water molecules and a beam of electromagnetic radiation.

B. Beam Propagation and the Beer-Lambert Law

Laser beam propagation though the atmosphere is described by Measures [1] to include all the processes that were mentioned previously; Rayleigh scattering, Mie scattering, Raman scattering, resonance scattering, fluorescence, absorption, and differential absorption and scattering. The summation of these contributions is described as the total attenuation along the path of propagation. This as-

sumes that any effects of spontaneous emissions or process that would add to the radiation are negligible. This absorption of the laser radiation is calculated using the Beer-Lambert law,

$$I(\nu, R) = I(\nu, 0) e^{-\int_0^R \kappa_\varepsilon(\nu, z) dz}, \tag{6}$$

where,

$I(\nu, R)$ is the final intensity of the laser radiation,

$I(\nu, 0)$ is the initial intensity of the laser radiation,

$\kappa_\varepsilon(\nu, z)$ is the total attenuation at distance z.

The total attenuation can be written as the summation of its components of elastic (Rayleigh) scattering, Raman scattering, absorption, and Mie volume attenuation.

$$\kappa_\varepsilon(\nu) = \sum \kappa_E(\nu) + \kappa_R(\nu) + \kappa_A(\nu) + \kappa_M(\nu), \tag{7}$$

where,

$\kappa_E(\nu)$ is the elastic scattering coefficient,

$\kappa_R(\nu)$ is the Raman scattering coefficient,

$\kappa_A(\nu)$ is the absorption coefficient,

$\kappa_M(\nu)$ is the Mie volume attenuation coefficient.

When considering the effects due to attenuation along a path in the atmosphere, the contribution from the absorption is typically of interest and can dominates over the other terms if the amount of inelastic scattering is small enough [1]. Scattering from large particles such as cloud, fog and haze particles cause the elastic scattering term to dominate and so for the laboratory environment it is assumed that particles of this size are not present. The absorption coefficient can be written in terms of the cross section.

$$\kappa_A(\nu, R) = N(R)\sigma^A(\nu), \tag{8}$$

where,

$N(R)$ is the number density from the molecular species of interest at range R,

$\sigma^A(\nu)$ is the molecules absorption cross section at wavenumber ν.

If the Beer-Lambert law can be rewritten to assume that the concentration along the path is constant then the integrated sum of the absorption coefficient will be a simple multiplication expression,

$$I(\nu, R) = I(\nu, 0)e^{-N\sigma^A(\nu)R}. \tag{9}$$

This equation is a simplified form of the Beer-Lambert equation (5) where several assumptions have been made. The absorption path for the laboratory experiment is 20 meters long and was in a controlled environment where these assumptions are valid. The cross section as derived previously combined with the Beer-Lambert law is,

$$I(\nu, R, p, T) = I(\nu, 0, p, T)e^{-N\cdot S_{\eta\eta}\cdot\frac{\gamma(p,T)}{\gamma(p,T)^2+\left[\nu-\nu^*_{\eta\eta}p\right]^2}\cdot R}. \tag{10}$$

This equation is quite bulky and not too usable; however it shows the complication that the cross section can have on laser beam radiation along a path. From Equation (8) the transmittance of the path is given as a ratio of the initial outgoing intensity to the final intensity. Finally, the Beer-Lambert law is used to determine the number density of the molecular species of interest from the cross section and the path length,

$$N = \frac{1}{\sigma^A(\nu)\cdot R}\ln\left\{\frac{I(\nu, R)}{I(\nu, 0)}\right\}. \tag{11}$$

This simple equation allows calculation of concentration from the ratio of the initial beam intensity and the final beam intensity.

In case the laser beam is a white light broad spectrum laser, then the easiest method to measure the beam energies separated into their wavelength components is to use an optical spectrometer. However, the spectrometer distorts the spectrum as described in the next section.

C. Measuring Data with a Grating Spectrometer

A grating spectrometer provides a spectral analysis of optical signals, but has a limited resolution. One limitation of a spectrometer is that it distorts the data because of the instrument function. Light entering the spectrometer through the entrance slit strikes a diffraction grating that generates a wavelength dependant diffraction pattern of minimums and maximums of light intensity. If the source contains many wavelengths of light then the grating spatially separates the different wavelengths for each diffraction order. The light reflects from the grating, satisfying the conditions for interference,

$$\sin\theta_m = \sin\theta_i + m\frac{\lambda}{d}, \tag{12}$$

where,

θ_m is the angle between normal of grating and order m reflection,

θ_i is the angle between normal of grating and incident light,

d is the distance between grating slits,

m is the diffraction order (integer).

The light is separated into its wavelength, or frequency, components as indicated in Figure 11.

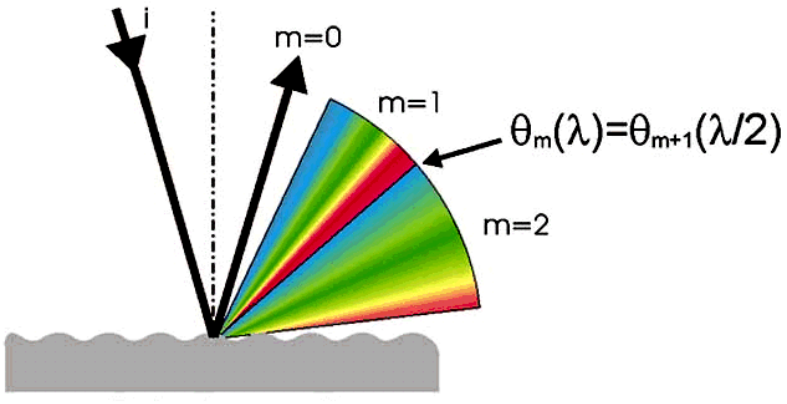

Figure 11: Polychromatic light diffracted from a grating [13].

The light diffracted from the grating is then refocused on an exit slit and a detector that is sensitive to the intensity of light is used to measure the intensity. Typically, the grating will rotate and thereby scan the various wavelengths past the exit slit. Some spectrometers will use a stationary grating and a scanning exit slit. In both cases the detector integrates the energy impinging upon it as the wavelengths are scanned. This combination of integration and spatial scanning is mathematically the convolution of the exit slit and the spectrum described by the voigt profile. Using the results from the Beer-Lambert law and this scanning mechanism of the spectrometer, the intensity recorded is represented in Equation (13),

$$I(\nu, R, N, \Delta\nu) = I_0 e^{-N\sigma^A(\nu)R} \otimes P(\nu, \Delta\nu), \tag{13}$$

where,

I_0 is the initial intensity,

$P(\nu, \Delta\nu)$ is the slit function.

Convolution of the functions is a nonlinear process that tends to smooth out the actual spectrum. This process can be demonstrated by modeling with the PcModwin software that utilizes the popular MODTRAN code. The transmittance of a 20 meter path in an environment of 37% relative humidity was modeled for different size slit function half widths. The slit function relates to the slits on the grating and the size of the exit slit. The plot in Figure 12 shows that the convolution of the slit function causes the smoothing of the spectrum.

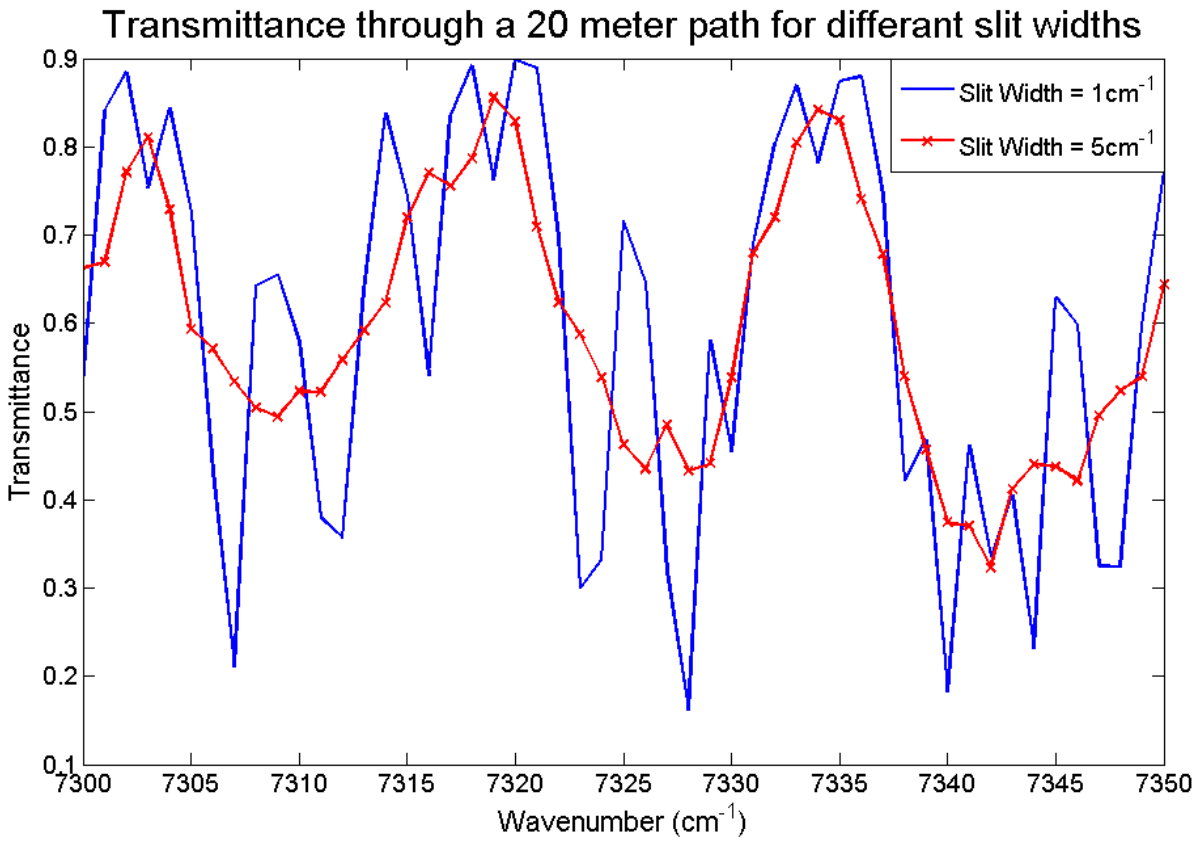

Figure 12: Transmittance curves generated using MODTRAN for two different size slit functions.

The resolving power of a spectrometer is given by,

$$R = \frac{\lambda}{(\Delta\lambda)_{\min}} = \frac{2Na \cdot \sin\theta_i}{\lambda}, \tag{14}$$

where,

$(\Delta\lambda)_{\min}$	is the least resolvable wavelength difference,
Na	is the grating width,
λ	is the mean wavelength (Hecht [14]).

Equation (14) assumes autocollimation where $\theta_i = -\theta_m = 90°$. At the limit of resolution the angular separation between the different frequencies is given by,

$$(\Delta\theta)_{\min} = \frac{(\Delta\lambda)_{\min} m}{a \cdot \cos\theta_m}. \tag{15}$$

This angular line width is due to the instrumental broadening and is inversely proportional to the width of the grating.

The simple grating spectrometer considered here is not the only kind of spectrometer used today. Some spectrometers use holographic gratings to spread the wavelengths and others use an array of photodetectors to measure the intensity as a function of wavelength. These spectrometers don't have to deal with the convolution of the spectrum; however they usually suffer a lower resolution and less sensitivity than a scanning type [13].

III. DATA ANALYSIS AND CONCENTRATION EXTRACTION

The relationship shown in Equation (13) is the calculated intensity equation that is used to correlate with the recorded spectrum. Here the $I(\nu,R,N,\Delta\nu)$ represents the expected wavelength variations that will be used to develop the quantitative analysis. Equation (13) can be manipulated several ways so to extract the concentration parameter. Analysis techniques are the focus of the next three sections, where first a more theoretical view is taken to invert the processing of the spectrometer and perform a deconvolution on the data. The second approach is to manipulate the equation to obtain a form that can be solved by advanced curve fitting methods using neural network approaches. Lastly, a technique is proposed where a simple least squares minimization of the ratio of minimum and maximum values are used to extract the concentration of the species being detected, in this case H_2O.

A. Deconvolution Method

The convolution analysis described above shows that the convolution of an instrument function of a spectrometer causes smoothing of the spectrum so that less features are observed. The reverse procedure of convolution is deconvolution and this method of data extraction was studied recently by Robert de Levie in his paper "On deconvolving spectra" [12]. First Levie assumes the recorded spectrum and the calculated spectrum can be described as a sum of Gaussian functions. Then he is able to show that simple math equations can be adjusted to deconvolve a Gaussian function. The difficulty in this approach will be shown to be equating the spectrum to a sum of Gaussian functions.

First Levie assumes the form of a measured spectrum is a Gaussian given by,

$$g_r = a_r e^{-\left[\frac{(t-c_r)}{2b_r}\right]^2} . \tag{16}$$

The same forms are assumed for the calculated, undistorted spectrum g_s, with the parameters a_s, b_s, c_s and a transfer function g_t, with parameters a_t, b_t, c_t. The transfer function in the case of a spectrometer is the slit function. Then to use this Gaussian approximation for a bandwidth of spectra, Levie assumes the measured spectra denoted as *r* can be written as,

$$r = \sum_{\nu} g_r . \tag{17}$$

The same approximation is made for the calculated spectrum *s* and a transfer function *t*. The goal is to find the sum of Gaussian functions for measured spectrum and a known instrument transfer function. The problem is to find the solution of the linear system so that $r = s \otimes t$, where the symbol $\otimes$ denotes convolution. The properties of the Fourier transforms can be applied to the convolution equation, written as $R = S \times T$ because a convolution operation transforms to a multiplication operation. Then to find the spectrum, s, the inverse convolution operation, must be performed, *s = rØt*. In the Fourier domain, this deconvolution is simply division, *S = R/T*. Once s is computed, the concentration can be extracted by using the Beer-Lambert law shown above to solve for *C,* where σ is the computed *s* spectrum. Levie has shown the deconvolution of two Gaussian functions is equal to a Gaussian where the parameters *a*, *b*, and *c* are related to the two original functions, and are calculated as,

$$c_s = c_r - c_t , \tag{18}$$

$$b_s = \sqrt{b_r^2 - b_t^2} , \tag{19}$$

$$a_s = \frac{a_r b_r}{a_t b_t b_s \sqrt{2\pi}} . \tag{20}$$

By using these parametric equations the complicated operation of deconvolution does not have to be performed. These parameters define one Gaussian curve to properly describe the spectrum. The number of Gaussian functions is equivalent to the number of lines that the molecule has in the wavelength range of interest.

The Gaussian approximation simplifies the process of finding the original spectrum; but the Gaussian curve fitting only approximates the spectrum. The initial assumption uses a Gaussian in place of a Lorentz lineshapes, and a comparison is shown in Figure 13 for a temperature and pressure broadened feature of water at 502.26cm^{-1}.

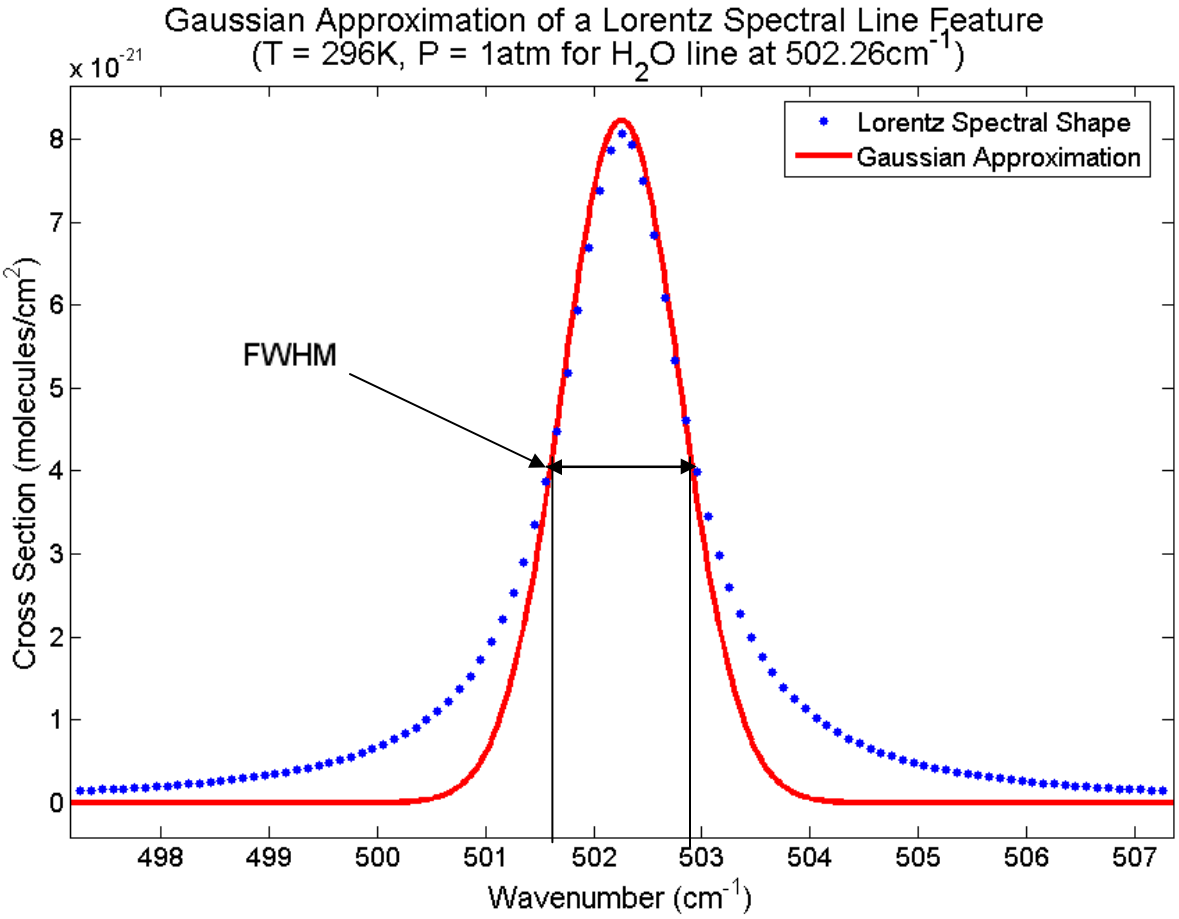

Figure 13: The Gaussian fitting to a single Lorentz line broadened spectrum.

Figure 13 shows that the Gaussian is a good approximation above the FWHM locations of the Lorentz function. This type of feature can be used to represent the continuous absorption as a sum of Gaussian functions and it should be a fair representation of the original. The Matlab curve fitting utility was

used to compare different numbers of Gaussian functions to fit the water absorption spectrum between 7050cm^{-1} and 7400cm^{-1} as shown in Figure 14.

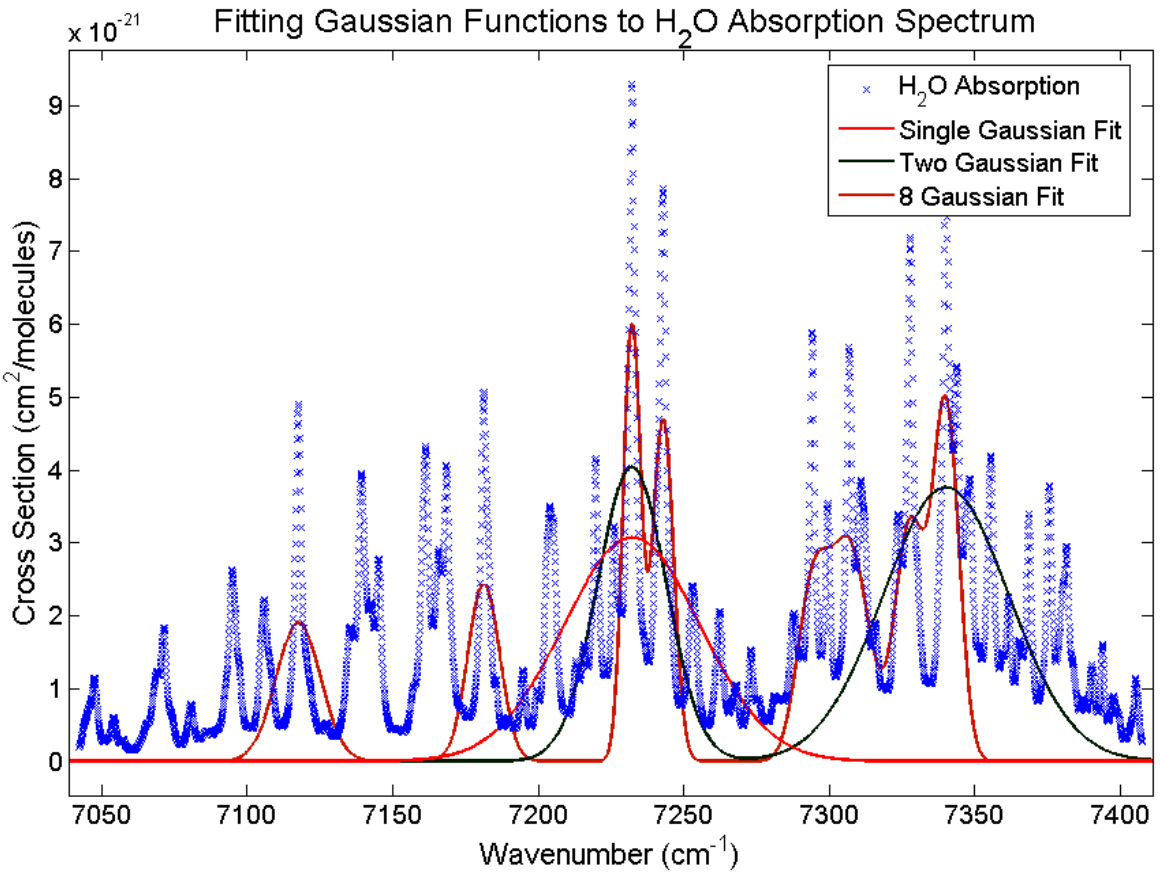

Figure 14: The Gaussian fitting to multiple spectral lines.

Figure 14 shows that the absorption peaks are better resolved as the number of Gaussian curves is increased. The result indicates that the Gaussian approximation method could be a good method for future measurements where the peaks are well separated. Comparisons to the absorption spectra are not provided by Levie; however these plots show good correlation. The drawback of this method is that a it will be difficult to represent a detailed spectrum, such as the water spectrum of interest, to a sum of Gaussian functions.

B. Levenberg-Marquardt Non-linear Fitting Algorithm

Another analysis technique was investigated by Stutz et al [3] which uses a nonlinear fitting algorithm for DOAS measurements of trace gas concentration. The Levenberg-Marquardt nonlinear fitting

procedure was also implemented by Tassou et al [2] to find a fitting parameter that correlates with the concentration of the detected species. It was shown that a reference spectrum is not needed when two absorption spectra sampled with two different slit functions. In this case, the nonlinear fitting algorithm is applied to the difference of the two sampled spectra and the result is a fitting parameter that corresponds to a concentration. The implementation of the Levenberg-Marquardt algorithm was not discussed in Tassou et al [2]. A brief review of neural networks is necessary to introduce the back propagating networks is given in the next section.

1) Introduction to Neural Networks: Neural Networks have been introduced to solve many computationally difficult problems. They have found applications in industries such as aerospace, automotive, medical, robotics and telecommunications to only name a few. Neural Network algorithms use parallel computing to solve computationally large problems. The increases in computer processing power have made these types of algorithms possible and feasible. One of the difficulties of the nonlinear neural networks is to defining a transfer function to describe the algorithm. It is sometimes difficult to understand what, if any, type of network is used to solve a certain problem. Testing and research have made neural network computing more inviting for many problems. A brief overview of neural networks background knowledge is presented here to show how Matlab's neural networks toolbox describes them. Howard Demuth and Mark Beale have written a textbook, "Neural Network Design", which is used as the reference for the Matlab help documentation "Neural Network Toolbox User's Guide," [15]. The use of the Levenberg-Marquardt algorithm can be viewed as a nonlinear curve fitting technique; however neural networks provide a more in depth understanding of the method described by Tassou et al. [2].

A neural network consists of many simple neurons connected in parallel, and computing outputs are based on the inputs and weights that give the system a target value for the desired result. If the target is not met, the network will adjust the weights and try again until it converges to the target value. A single neuron's operation is quite simple; however when connecting to a large group of neurons that iteratively adjust their weights, these neurons can prove to be computationally powerful. A neuron circuit is shown in Figure 15.

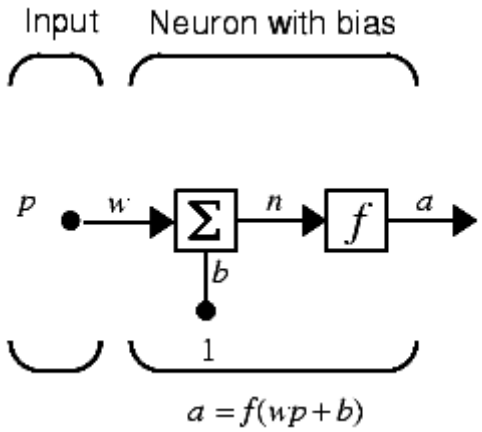

Figure 15: A simple neuron circuit [15].

The output is given as shown in Figure 15 where,

- a is the output,
- f is the transfer function,
- w is the weighting values,
- p is the input,
- b is the biased offset.

Simple linear feedfoward networks, f, use a transfer function defined as unit step function, a linear function, or logsig function. Each operates on the weightings and the input to achieve different outputs depending on the desired result and the type of system that is modeled. The simple diagram shows a single input, but this is not usually the case. Figure 16 shows the case where the input is an array with different weightings for each input, supplied by a weighting array.

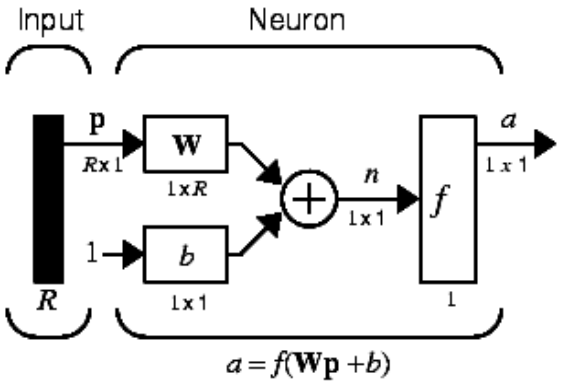

Figure 16: A neuron circuit for multiple inputs [15].

Now, **W** is an array of 1 x R elements and **p** is an array of Rx1 elements, and *b* is still a scalar. The output *a* is also still a scalar for this circuit because the result of **Wp** is a scalar from vector multiplication. Now to continue to build a conceptual neuron circuit, we next consider that multiple neuron circuits use an array of inputs with different weight supplied by a weighting array. Each neuron circuit will have its on bias and each will produce their own output. The circuit is shown in Figure 17.

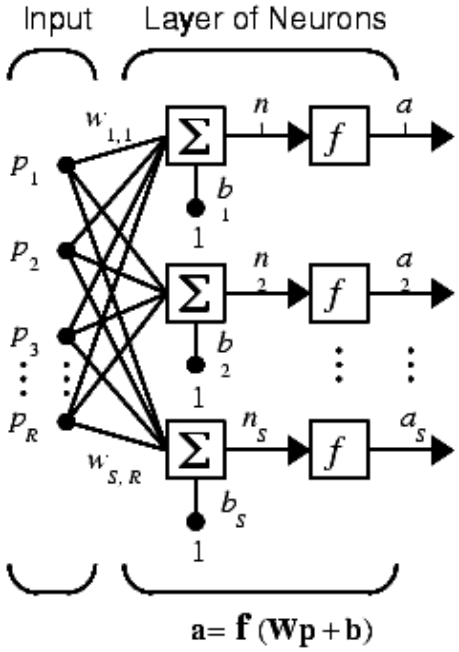

Figure 17: A layer of neuron circuits with multiple inputs and multiple outputs [15].

Now, all the parameters of the neuron equation shown in Figure 17 are arrays or matrices. This circuit can now define what is called a layer of neurons. The diagram in Figure 18 is provided to show a simplified matrix view of the circuit shown in Figure 17.

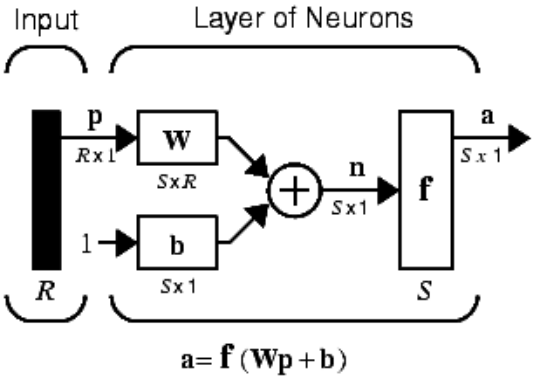

Figure 18: A simplified layer circuit [15].

This last neural circuit diagram show a simple feedfoward neural network system in a dynamic mode that operate iteratively to update the weighting matrix and bias array to reach a desired target. The ability for the network to update the weighting and biases is only a character of unsupervised, adaptive networks. The feedback control to readjust the weights is accomplished by calculating an error. The error is defined as,

$$e = t - a\,. \tag{21}$$

The error is defined as the difference of the targets and the outputs and is used to define a learning rule to modify the weights and biases. The simplest learning rule to realize is that of a perceptron,

$$W^{new} = W^{old} + e \cdot p^{T}\,, \tag{22}$$

$$b^{new} = b^{old} + e\,. \tag{23}$$

2) Backward Propagating Networks: The term back propagation refers to the manner in which the gradient is computed for nonlinear multilayer networks. The simplest implementation of back

propagation learning updates the network weights and biases in the direction in which the performance function decreases most rapidly - the negative of the gradient. A single iteration of the back propagating algorithm is written as,

$$x_{k+1} = x_k - \alpha_k g_k , \tag{24}$$

where,

α_k is the learning rate,

g_k is the current gradient,

x_k is the vector of current weights and biases.

Quasi-Newton Algorithms have $\alpha_k = A_k^{-1}$; where A_k is the Hessian matrix, the second derivatives of the performance index at the current values of the weights and biases. The Quasi-Newton method approximates the Hessian matrix to optimize time.

$$\mathrm{H}(f)_{ij}(x) = D_i D_j f(x). \tag{25}$$

The Levenberg-Marquardt uses the Jacobian matrix to approximate the Hessian matrix. The equation for the Levenberg-Marquardt is,

$$x_{k+1} = x_k - \left[J^T J + \mu I\right]^{-1} J^T e . \tag{26}$$

J is the Jacobian matrix that contains first derivatives of the network errors with respect to the weights and biases, and e is a vector of network errors or the difference between the targets and the outputs. Matlab provides a user friendly environment to prepare these types of neural networks where only the inputs and target values are needed.

These nonlinear adaptive learning algorithms may prove to have applications for remote sensing where it is difficult to retrieve certain parameters. Tassou et al [2] show that with some manipulation of the Beer-Lambert law, and with an extra measurement using another slit width, the Levenberg-Marquardt adaptive learning algorithm can be used as a nonlinear fitting method and concentration can be ex-

tracted. The following equation shows the difference of the two measurements where two slit sizes were used and the concentration can be factored out as,

$$F(a_1,\lambda) - F(a_2,\lambda) = C_i\left[F_i(a_1,\lambda) - F_i(a_2,\lambda)\right], \tag{27}$$

where,

$F(a_{1,2},\lambda)$ is the measure experimental spectra (a_1 and a_2 denote the use of different gate functions with width a_1 and a_2 respectively),

$F_i(a_{1,2},\lambda)$ is the reference spectra for i^{th} species,

C_i is the concentration of the i^{th} species.

Although the process of applying the Levenberg-Marquardt algorithm was not discussed by Tassou et al. [2], the inputs would be the reference spectra, $F_i(a_{1,2},\lambda)$, and the target values would be the measure data, $F(a_{1,2},\lambda)$. The corresponding weights would adjust to find the concentration C_i. Figures 19 and 20 are the results of the study by Tassou, et al. [2] and show the training of the Levenberg-Marquardt algorithm.

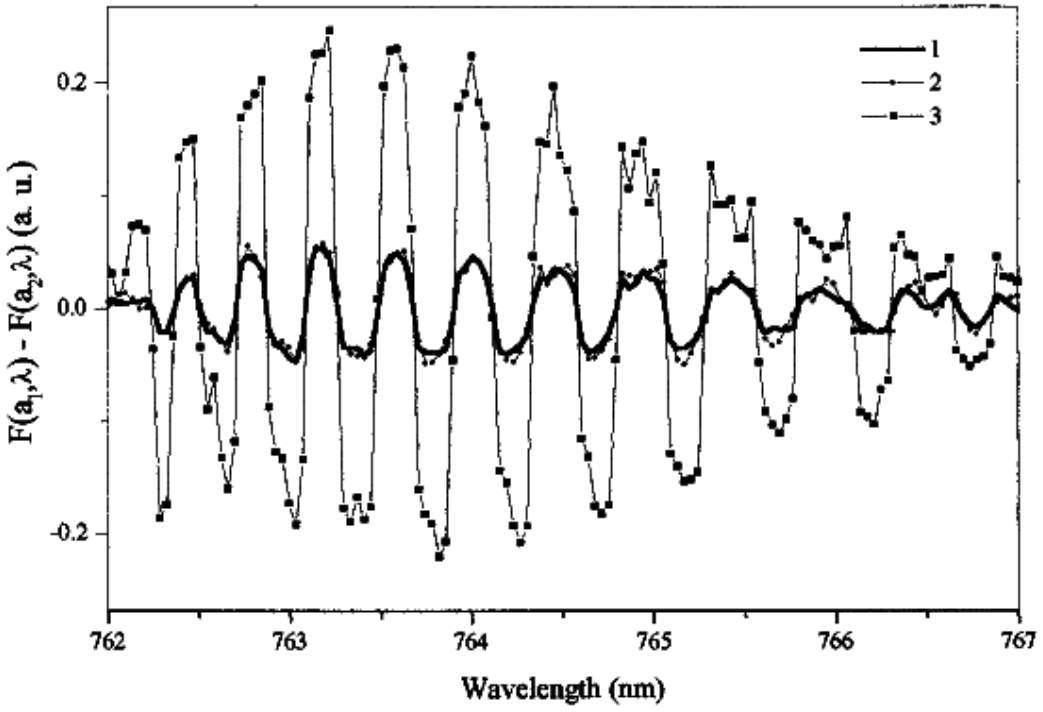

Figure 19: Results of the nonlinear curve fitting in progress given by Tassou et al. [2]

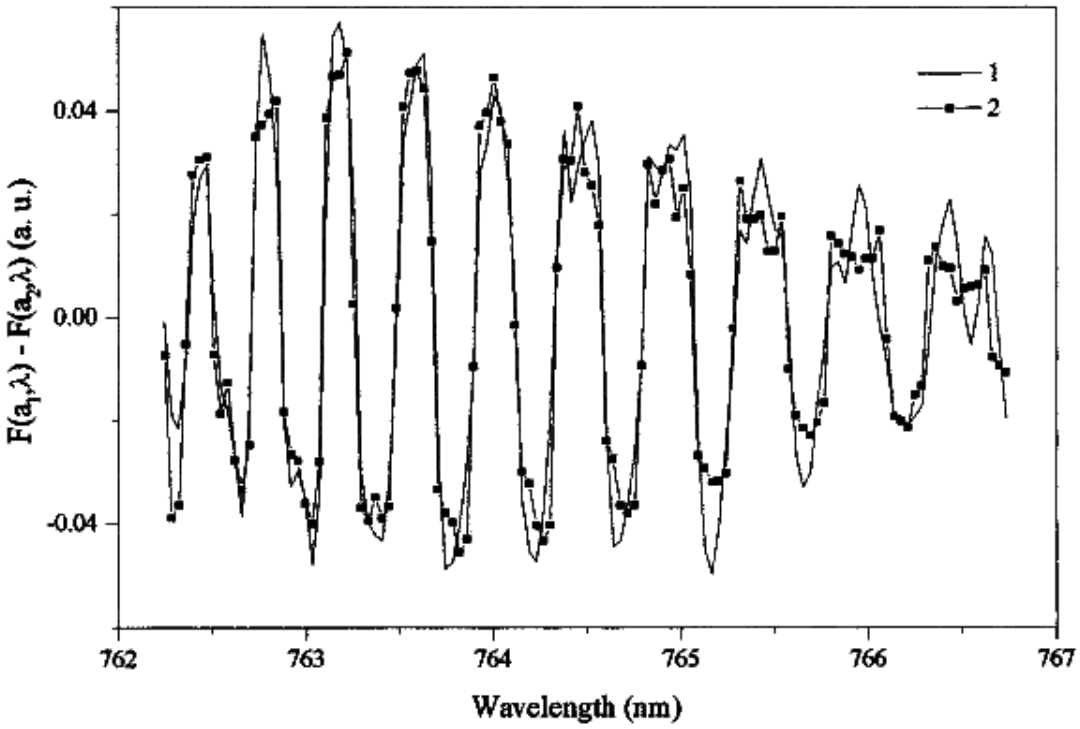

Figure 20: Final results of the nonlinear curve fit given by Tassou et al. [2]

The nonlinear fit of the data gives a robust method, however two experiments must be run, and the experimental error is not clearly defined by the fitting error.

C. Ratio Method

This investigation will focus on describing the absorption spectrum as a function of relative humidity to develop a new method to quantify the amount of water vapor through the path. The simulation software tool, PcModwin was used to analyze the spectrum structure and how it changes as water concentration increases on the path. PcModwin incorporates the widely used MODTRAN code for optical atmospheric analysis. PcModwin also incorporates the effects of the convolution of a spectrometer's slit function on the data. The environmental input for the MODTRAN code was calculated to simulate the same atmosphere as seen in the experiment. The simulation was computed for different values of relative humidity and examples from a few of the simulations are shown in Figure 21.

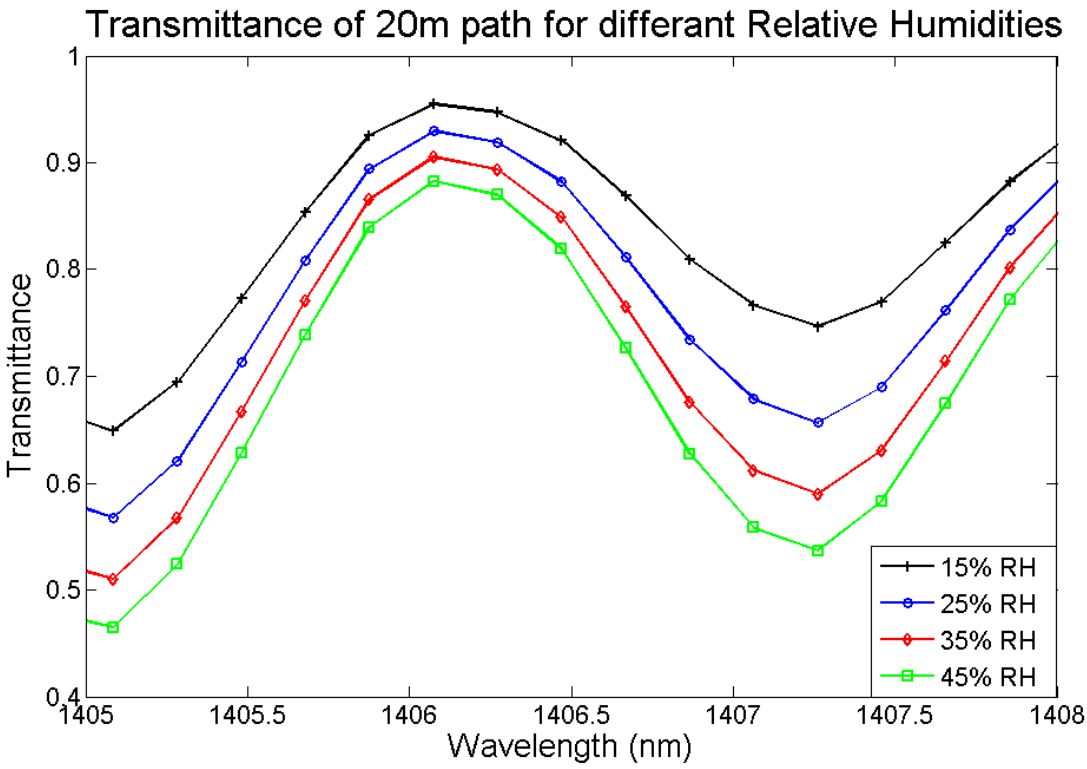

Figure 21: MODTRAN plots of different relativities from 15% to 45% RH.

These simulations show the expected decrease in transmittance as relative humidity increased. However, our objective is to quantify a parameter for each curve that would differentiate it from the other curves for relative humidity. Such a parameter is the ratio of a relative minimum to a specific adjacent relative maximum. Simulations show the uniqueness of this ratio parameter in Figure 21, and in the summary of Table 1.

Table 1: Ratios for different Relative Humidity

Relative Humidity	Min at 1407.3nm	Max at 1406.1nm	Ratio (Min/Max)
15%	0.7469	0.95506	0.7821
25%	0.65684	0.9294	0.7067
35%	0.58973	0.9053	0.6514
45%	0.53676	0.88256	0.6082

Table 1 shows that each relative humidity curves can be characterized by a unique ratio of relative minimum to maximum. This ratio can be calculated for every relative minimum and maximum that is in the spectrum of water vapor between 1350 nm and 1420 nm. To understand the relation between each ratio and relative humidity the plot in Figure 22 is shown.

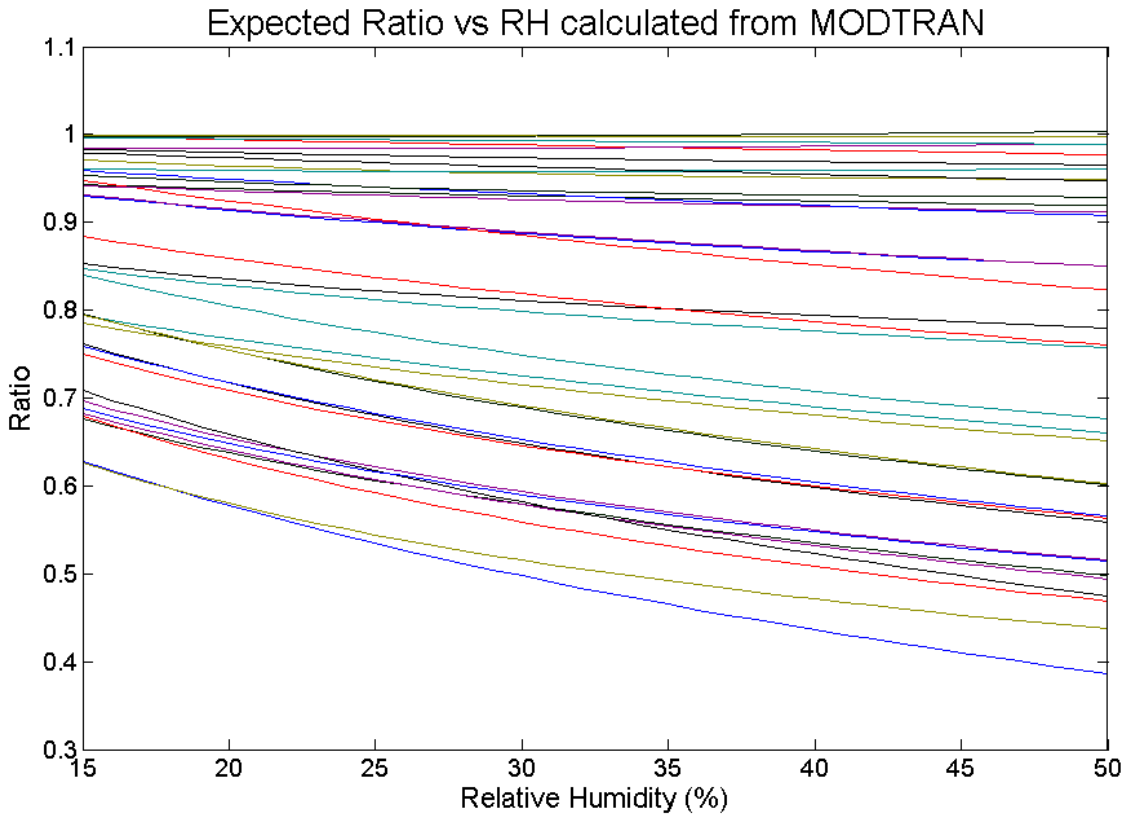

Figure 22: 36 Peak selections plotted versus relative humidity.

The plot of Figure 22 shows some peak pairs have a larger slope than others as the concentration of water is increased along the path. This difference in slope can be attributed to the fact that with in the resolution steps of the spectrometer, different amounts of spectral lines are adding to the attenuation. For example in Figure 9, between 7065 cm^{-1} and 7075 cm^{-1} there are more spectral features contributing to the absorption by water than there are between 7075 cm^{-1} and 7085 cm^{-1}. This means that the calculated ratios only correspond to measurements that are taken by a spectrometer that has the same instrument function as what was used in PcModwin. The 36 peak ratios are found using a peak finding algorithm implemented in Matlab and the plot in Figure 23 shows a section of the results.

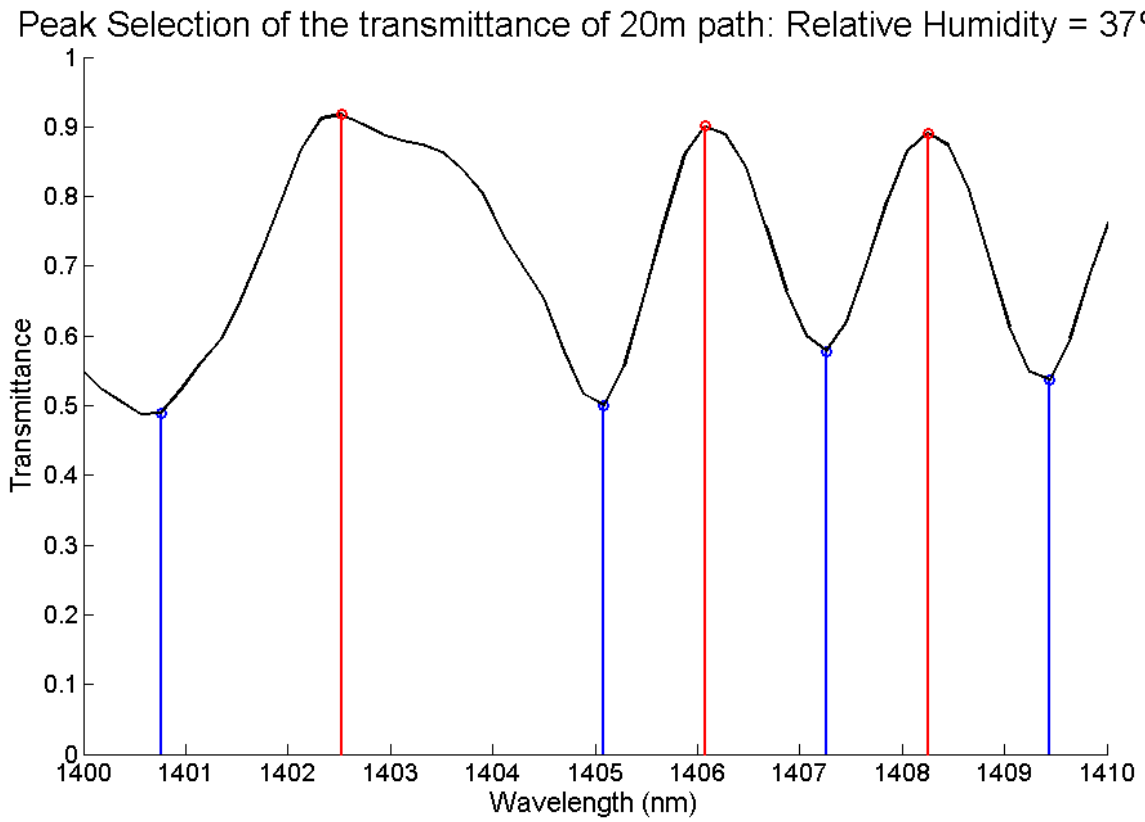

Figure 23: Peak selection of the MODTRAN reference plot.

These ratios are used to compare the measured data to the simulation values. The closeness of the maximum and minimum wavelengths provide a method to cancel out any wavelength dependencies that has corrupted the measured data assuming that the wavelength dependencies vary slow over the wavelengths.

1) Experiment: The experiment was conducted in an environmentally controlled laboratory where the relative humidity was measured using a sling psychrometer and found to be 37% at 72° F. The schematic in Figure 2 shows optical layout of the experiment. Sub-nanosecond laser pulses from a passively Q switched microchip laser (JDSU NP-10620-100, wavelength at 1064nm, average power ~ 40mW) are coupled into a 2 cm long photonic crystal fiber (Blaze Photonics SC-5.0-1040) to generate super-continuum white light. The white light is collimated and propagates along a path of 20 meters in the air and then is collected and measured by an optical spectrum analyzer (Ando AQ6315E) as shown in Figure 23.

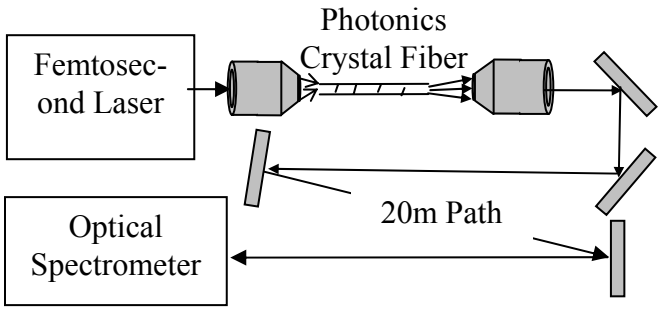

Figure 24: Experimental Setup.

2) Results: The data recorded from the spectrometer was not normalized and was scaled to be plotted along with the calculated spectrum from the simulation to visually determine the correlation of the spectrum, see Figure 25.

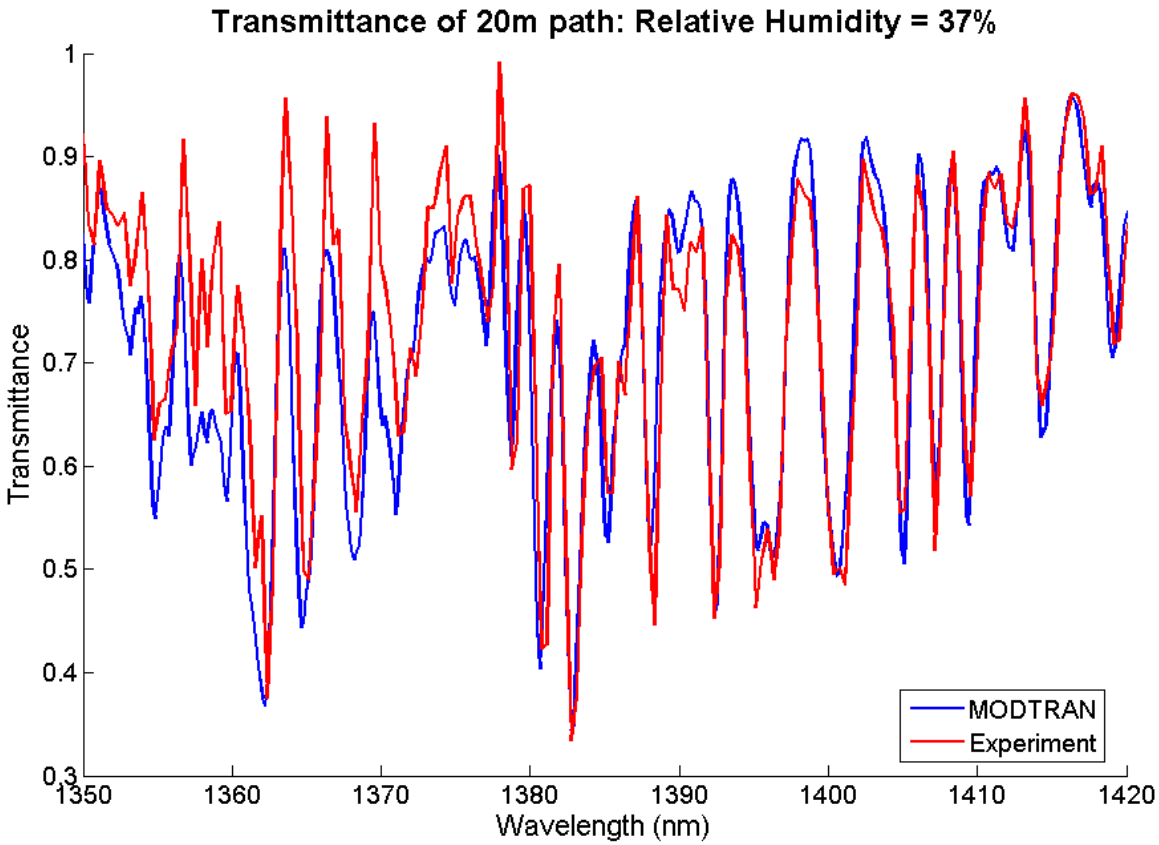

Figure 25: The experimentally measured spectrum compared with the calculated spectrum from PcModwin at 37% RH.

The least squares error is calculated as,

$$R^2 = \sum \left(R_i^M - R_i^T \right)^2 , \tag{28}$$

where, R_i^M is the measured spectrum data, R_i^T is the theoretical spectral data. A value for R^2 is calculated for each simulation and the smallest R^2 value is selected as the measured relative humidity. Figure 25 shows the minimization of the R^2 parameter.

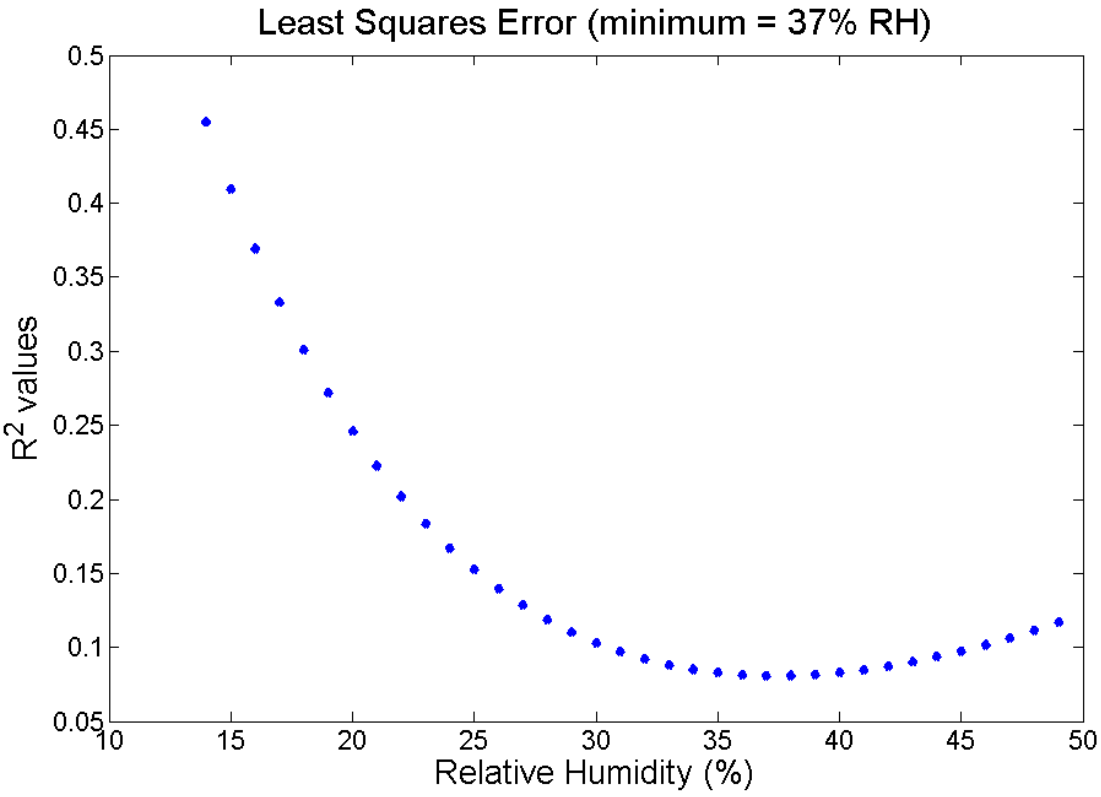

Figure 26: Least squares error for each relative humidity that was simulated.

Each ratio can be considered a different experiment so that the error of the experiment is,

$$Error = R_i^M - R_i^{T_{37\%}} , \tag{29}$$

For each 36 ratios an error bar is calculated from the equation above and is plotted in Figure 27.

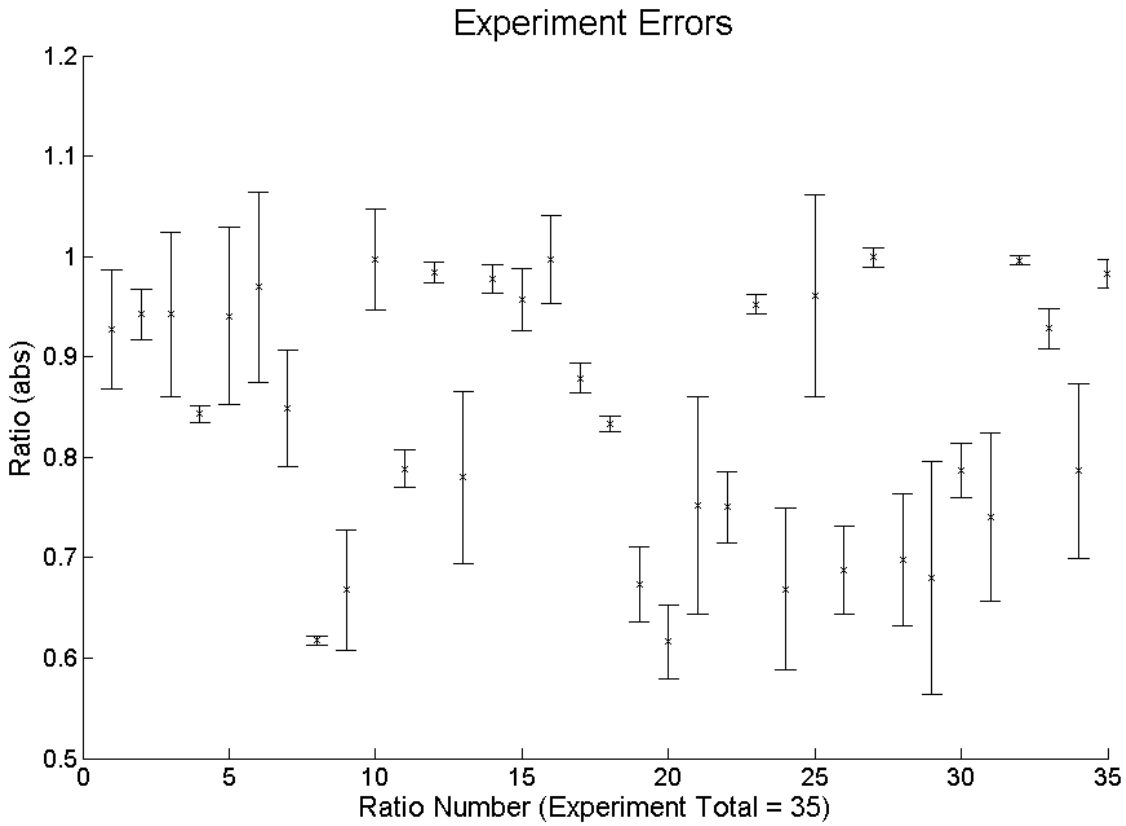

Figure 27: Error bars for each ratio experiment.

The variance of the 35 peak ratios is given as,

$$Var = \sum \frac{R^2}{N-1} = \frac{0.0808}{34} = 0.0024 \qquad (30)$$

The value N in the equation above is the number of ratios, or samples, for the experiment. This variance corresponds to a relative humidity in the laboratory of 37%+/-0.8%RH.

3) Discussion: This experiment provides a new method to quantify a species under investigation. The method described above was developed by looking at the character of the spectrum as it changes with a measured parameter such as relative humidity. This same technique can also be accomplished using a density of water vapor because it is provided as an input into the PcModwin simulation software. Our technique used a direct method of curve fitting or curve matching that utilizes the peaks and valleys of the absorption spectrum to quantify relative humidity. The ability to quantify a species from the long path absorption spectrum shows the feasibility to use a supercontinuum white light laser for

laser remote sensing applications. Further experimentation will continue to fine tune the process and detect smaller absorption features of water. Other constitutes such as O_2, CO_2 and possible NO_2 will be included in future investigations.

IV. CONCLUSION

The analysis techniques that were provided here show three different approaches to determine the concentration of a species from a large bandwidth spectrum. The convolution process from the Doppler broadening and instrument function broadening of the spectrometer make it difficult to extract data such as concentration from a direct comparison to the calculated spectrum using the HITRAN database. The first method discussed presented by Levie [12], shows a process of fitting many Gaussian function to approximate the desired spectrum. This method would be too computationally difficult to conduct when the spectrum under investigation has many features. The second analysis method gives a nonlinear fitting technique to find the concentration of a species from a measure spectrum. This technique requires two spectrometer measurements with two different size slits. This might require a system to have multiple spectrometers to be sure two measurements are attained within a close time period. The final technique presented here gives a straight forward easy approach to attain the concentration or relative humidity from measured spectral data. There seems to be some fluctuation in the errors of each peak ratio. The peak ratio method is dependant upon the spectrometers instrument function. The calculated spectrum from PcModwin will have to be recalculated for different instrument functions of the spectrometer.

The integration of a femtosecond pulsed generated white light laser will have an exponential effect on the types of measurements a lidar system will have. The 0.2μm to 1.7μm broadband ability of the Penn State femtosecond pulsed white light laser will give the ability to develop the concept for atmospheric remote sensing. Some unique measurements that a white light lidar system will provide are number density, size distribution and refractive index of aerosol particles. It also, will give the opportunity to use SPR-DIAL (Spectral Pattern Recognition – Differential Absorption Lidar) techniques to perform spectral analysis of chemical species. The experiment and analysis provide in this study are to make the first developments in this area of SPR-DIAL. Future experiments should test the feasibility of the methods offered here and apply these methods to data from an uncontrolled atmosphere such as one in open air and for a much longer path.

REFERENCES

[1] Measures, R. M., *Laser Remote Sensing Fundamentals and Applications*, Krieger Publishing Company, Malabar, Fl., 1984.

[2] Tassou, M, Przygodzki, H., Delbarre, H., Boucher, D., "Atmospheric Gas Detection with Broadband Sources," International Journal of Infrared and Millimeter Waves, Vol. 23, No. 8, 1227-1239, August 2002.

[3] Stutz, J, Platt, U., "Numerical Analysis and Estimation of the Statistical Error of Differential Optical Absorbtion Spectroscopy Measurements with Least-Squares Methods," Applied Optics, Vol. 35, No. 30, 6041-6053

[4] Hagan M. T., Menhaj, M. B., "Training Feedfoward Networks with the Marquardt Algorithm," IEEE Transactions on Neural Networks, Vol. 5, No. 6, pp. 989-993, November 1994

[5] J.C. Knight, T.A. Birks, P.S. Russell and D.M. Atkin, ²All-silica single-mode optical fiber with photonic crystal cladding,² *Opt. Lett.* 21, 1547-1549, 1996.

[6] Fedotov, A.B., Zheltikov, A. M., Mel'nikov, L. A., Tarasevitch, A. P., von der Linde, D., "Spectral Broadening of Femtosecond Laser Pulses in Fibers with a Photonic-Crystal Cladding," JETP Letters, Vol. 71, No. 7, pp.281-284, 2000.

[7] Wille, H., Rodriguez, M., Kasparian, J., Mondelain, D., Yu, J.,Mysyrowicsz, A., Sauerbrey, R., Wolf, J.P., Woste,L., "Teramobile: A mobile femtosecond-terawatt laser and detection system," Eur. Phys. J. Applied Physics, Vol. 20, pp. 183-190, 2002.

[8] Mejean, G., Bourayou, R., Kasparian, J., Rodriguez, M., Salmon, E., Yu, J., Lehmann, H., Stecklum, B., Laux, U., Eisloffel, J., Scholz, A., Hatzes, A.P., Sauerbrey, R., Woste, L., Wolf, A.P., "Femtosecond White-Light Lidar for Simultaneous Cloud Particle Sizing and Humidity Measurements," Presented at the 22nd International Laser Radar Conference (ILRC22), Matera, Italy, 2004.

[9] Liu, Z., Shi, K., Peng, L., White light laser (Supercontinuum), University Park, PA, [Online], Available: http://ultrafastoptics.ee.psu.edu

[10] Atkins, P.W., "Physical Chemistry," Fourth Edition, W. H. Freeman and Company, New York, 1990.

[11] McClatchey, R. A., Benedict, W. S., Clough, S. A., Burch, D. E., Calfee, R. F., Fox, K., Rothman, L.S., Garing, J. S., "AFCRL Atmospheric Absorption Line Parameters Compilation," Environmental Research Papers, No. 434, January 1973.

[12] Levie, R., "On Deconvolving Spectra," Am. J. Phys., Vol. 72, No. 7, pp. 910-915, July 2004

[13] http://www.getspec.com

[14] Hecht, E., "Optics," Fourth Edition, Addison Wesley, 1301 Sansome St., San Francisco, CA 94111, 2002.

[15] Demuth, H., Beale, M., "Neural Network Toolbox User's Guide," Version 4, The MathWorks, Inc., 3 Apple Hill Drive, Natick, MA, 1992.

[16] http://pclasim47.univ-lyon1.fr/teramobile.html

[17] K. Shi, P. Li, S. Yin, and Z. Liu, "Chromatic confocal microscopy using supercontinuum light, "*Optics Express* **12**, 2096-2101(2004)